# Applicability of Dynamic Facilitation Theory to Binary Hard Disk Systems

Masaharu Isobe*
*Graduate School of Engineering, Nagoya Institute of Technology, Nagoya, 466-8555, Japan*

Aaron S. Keys and David Chandler
*Department of Chemistry, University of California, Berkeley, California 94720, USA*

Juan P. Garrahan
*School of Physics and Astronomy, University of Nottingham, Nottingham NG7 2RD, United Kingdom*
(Received 15 April 2016; published 28 September 2016)

We numerically investigate the applicability of dynamic facilitation (DF) theory for glass-forming binary hard disk systems where supercompression is controlled by pressure. By using novel efficient algorithms for hard disks, we are able to generate equilibrium supercompressed states in an additive nonequimolar binary mixture, where microcrystallization and size segregation do not emerge at high average packing fractions. Above an onset pressure where collective heterogeneous relaxation sets in, we find that relaxation times are well described by a "parabolic law" with pressure. We identify excitations, or soft spots, that give rise to structural relaxation and find that they are spatially localized, their average concentration decays exponentially with pressure, and their associated energy scale is logarithmic in the excitation size. These observations are consistent with the predictions of DF generalized to systems controlled by pressure rather than temperature.

DOI: 10.1103/PhysRevLett.117.145701

It is highly debated which of the competing theoretical approaches to the glass transition is the most appropriate for describing the relaxational dynamics of glass formers [1–6]. One perspective is provided by so-called dynamic facilitation (DF) theory [4] which is based on the detailed study [7–10] of idealized kinetically constrained models (KCMs) [11]. The central predictions from DF are as follows. (i) In the supercooled regime relaxation originates from localized excitations or soft spots distributed randomly with a concentration that decreases exponentially with inverse temperature; their kinetics is facilitated (excitations allow for relaxation in their vicinity), giving rise to heterogeneous dynamics [4]. Excitations are explicit in KCMs, but in actual glass formers, they would be emergent [4]. (ii) Relaxation is "hierarchical" (as in the East facilitated model [12,13] or its generalizations [11]) leading to an overall relaxation time that follows a "parabolic" law [14], i.e., the exponential of a quadratic function of inverse temperature, which while super-Arrhenius is distinct from the empirical Vögel-Fulcher-Tammann law [1–6], in particular as it has no finite temperature singularity. (iii) The underlying glassy slowing down is a nonequilibrium "space-time" transition [9,10] whose fluctuations manifest as dynamic heterogeneity.

The above predictions of DF have been seen to hold in thermal atomistic systems: Effective excitations can be identified [15,16] through path sampling techniques [17,18] and are found to conform to (i) above; the parabolic law (ii) is an adequate description of relaxation rates at low temperature for experimental liquids [14]; and active-inactive transitions (iii) are, indeed, found in simulations of atomistic liquids by means of large deviation techniques [19,20]. Here, we extend the DF approach to systems where the controlling parameter is pressure, exploring, in detail, the validity of predictions (i) and (ii) for binary hard disks. While there can be differences in specific aspects of the dynamics between dense systems in dimensions two and three [21] (and even more significantly on their thermodynamics), here, we are interested in general properties of slow relaxation under supercompressed conditions—two-dimensional systems are a useful test ground as they can be studied exhaustively, as we describe below.

In systems of hard particles, the primary control parameter is either the pressure $p$ or the packing fraction $\nu$. In analogy with the thermal problem, we will consider the case where pressure is the control parameter. We make natural extensions of the basic DF scaling relations. First, prediction (i) implies that the density of excitations $c_a$, where $a$ is the size of particle displacement used to identify an excitation (see below), goes as

$$c_a \propto \exp\left[-\kappa_a(p^* - p_0^*)\right]. \tag{1}$$

Here, $p^*$ is the reduced pressure $p^* = \beta p \sigma_*^2$, where $\sigma_*$ is the effective diameter in a binary mixture [22], with inverse temperature $\beta = 1/k_B T$ and $k_B$ the Boltzmann constant. In Eq. (1), $p_0^*$ is the onset pressure above which cooperative and heterogeneous dynamics becomes significant (setting the regime of validity of the DF approach). Furthermore,

 

the scale $\kappa_a$ associated to a displacement of size $a$ should grow logarithmically as

$$\kappa_a - \kappa_{a'} = \gamma \kappa_{\sigma_*} \ln (a/a'), \tag{2}$$

where $\gamma$ is a nonuniversal exponent of order unity, and $\kappa_{a'}$ and $\kappa_{\sigma_*}$ are $\kappa_a$ at $a = a'$ and $a = \sigma_*$, respectively. Similarly, for (ii), we have that the primary relaxation time, $\tau_\alpha$, should be the exponential of a parabolic function of the reduced pressure

$$\tau_\alpha = \tau_0 \exp [\kappa^2 (p^* - p_0^*)^2], \tag{3}$$

with $\kappa$ a system specific activation scale. Equations (1), (2), and (3) are the equivalents of the DF scaling forms to those applicable to soft interactions, see Refs. [14,15].

We consider $N$ additive binary hard disks, of small and large diameters $\sigma_0$ and $\sigma_1$, and mole fractions $x_0$ and $x_1$, respectively. The size ratio is $\alpha = \sigma_1/\sigma_0$, and the system is in a $L_x \times L_y (= A)$ square box ($L_y/L_x = 1$) with periodic boundaries. We aim to establish, at high densities, true equilibrium where the equilibrium distribution can be reached from any initial condition. Given that structural relaxation becomes extremely slow at high densities, to accelerate equilibration, we use an efficient algorithm based on event-chain Monte Carlo (ECMC) calculations [23]. The equilibrium state obtained by ECMC calculations is exactly equivalent to that obtained via event-driven molecular dynamics (EDMD) [24] but is reached much faster than with conventional MC calculations or EDMD, especially in large and dense systems. (For a comparison of CPU times see Refs. [25,26]).

The system is prepared for each packing fraction, $\nu = N\pi(x_0\sigma_0^2 + x_1\sigma_1^2)/(4A)$, initially in equilibrium by performing long runs with ECMC for up to $\mathcal{O}(10^{13})$ collisions. After equilibration, production runs for equilibrium dynamics are done using EDMD. Particle numbers are either $N = 32 \times 32$ or $N = 64 \times 64$, and packing fractions vary from $\nu = 0.30$ to $\nu = 0.80$. The units are set by the mass $m$, the effective diameter $\sigma_*$ [22], and energy $1/\beta$.

Figure 1 shows the phase diagram, via the equation of state (EOS) of the binary mixture hard disk system as generated with ECMC and EDMD, for size ratio $\alpha = 1.0$, 1.11, 1.15, 1.2, 1.4 for an equimolar mixture, $x_1 = 1/2$, and a nonequimolar mixture, $x_1 = 1/3$ (see, also, Ref. [27] for simulation details). The reduced pressure $p^*$ in terms of the packing fraction $\nu$ is calculated by the virial form of collisions in EDMD [30]. In the liquid regions ($\nu < 0.69$), the pressure for different values of the parameters coincides with the universal liquid branch curve. Above $\nu > 0.70$, a phase transition occurs in the monodisperse system ($\alpha = 1$) [25,31,32]. With increasing $\alpha$, the coexistence region ($0.70 < \nu < 0.72$) between liquid and crystal gradually shrinks and shifts toward higher densities and pressures, almost disappearing at $\alpha > 1.3$.

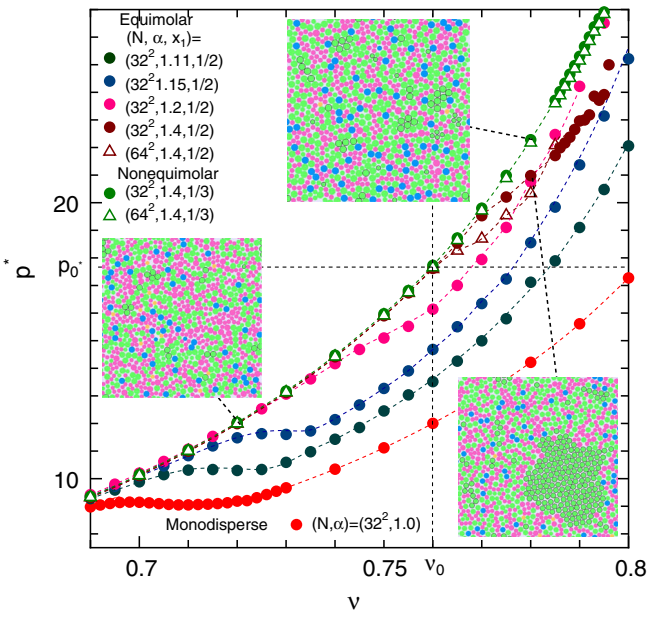


FIG. 1. Phase diagram of hard disk binary mixtures [27] in terms of the EOS. Insets show examples of equilibrium configurations: for the nonequimolar mixture with $(N, \alpha, x_1) = (32 \times 32, 1.4, 1/3)$, we show a typical liquid configuration at $\nu = 0.720$, and a typical supercompressed configuration at $\nu = 0.780$. In contrast, for the equimolar mixture $(N,\alpha,x_1) = (32\times32,1.4,1/2)$, at $\nu = 0.780$, typical configurations show microcrystallization of 40% large disks immersed in the amorphous phase. Note that, when $x_1$ is decreased below $x_1 = 1/3$, microcrystallization of small disks emerges. Disks are colored by the number of nearest neighbors detected by a 2D version of the solid-angle based nearest-neighbor (SANN) algorithm [28] as 4 (orange), 5 (pink), 6 (green), 7 (blue), and 8 (dark blue). Disks belonging to a crystal cluster [29] are also indicated by a black perimeter.

Overall, we find four phases: an amorphous liquid, a pure crystal (only in the monodisperse case $\alpha = 1$), a mixed crystal [33], and a crystal-amorphous composite phase. For an equimolar binary mixture $(\alpha, x_1) = (1.4, 1/2)$, when $\nu \geq \nu_0$, with $\nu_0$ being an onset packing fraction, all final configurations show microcrystallization of large disks immersed in the amorphous state, instead of a pure amorphous state. This is a slow coarsening process in which a crystal cluster emerges spontaneously, and sufficiently long simulation times are required to observe it (order of $10^{12}$ to $10^{13}$ collisions) in ECMC [34]. (Our EOS is compatible with that found in Ref. [35] using Metropolis MC, for times $\sim 4 \times 10^9$ trial moves in systems of size $N = 400$, although our systems are larger, and we simulate for much longer times.) Above $\nu \sim 0.8$, the relaxation time is too large to observe equilibrium behavior in our simulations.

It is worth remarking that the equimolar mixture at $\alpha \sim 1.3$ was believed not to crystallize or demix [36,37], thus, being studied extensively as a two-dimensional glass former. Subsequent work showed that, in the supercompressed region, this system had no ideal glass transition

[38,39], and that true equilibrium was a stable crystal-amorphous composite (as in binary equimolar soft disks [40,41]). Previous simulations had not been able to observe spontaneous crystallization since the coexistence is difficult to realize directly due to surface tension between phases in small systems, and since diffusion of large disks towards nucleation is kinetically strongly suppressed [39,42].

Typical configurations are shown as insets in Fig. 1. For a nonequimolar binary mixture at $(\alpha, x_1) = (1.4, 1/3)$, a smooth continuous crossover from the normal liquid ($p^* < p_0^*$) to the supercompressed one ($p^* > p_0^*$) is observed, where $p_0^* \approx 17.66$. Above the freezing point of large disks ($p_f \approx 19.7$), the pressure in the equimolar case is lower than that of the nonequimolar due to microcrystallization. Partial freezing of large hard disks above the freezing packing fraction, $\nu_f \approx 0.77$, also gives rise to a size dependence of pressure due to finite size effects on the surface tension of microcrystallization.

The equilibrium phase diagram of Fig. 1 suggests that $(\alpha, x_1) = (1.4, 1/3)$ is a suitable system for studying features associated with glassy slowing down, as amorphous supercooled states can be prepared in equilibrium at supercompressed conditions of $p^* > p_0^*$. Hereafter, we focus on the model with $(N, \alpha, x_1) = (64 \times 64, 1.4, 1/3)$ to investigate the accuracy of DF predictions to the dynamics of the hard disk binary mixture.

First, we consider the identification of excitations. We follow the procedure of Ref. [15] (see, also, [16]). We can quantify the overall density of excitations with the indicator function

$$C_a(\Delta t) = \frac{1}{N}\sum_{i=1}^{N} \theta[|\overline{\mathbf{r}}_i(\Delta t) - \overline{\mathbf{r}}_i(0)| - a], \qquad (4)$$

where $\theta$ is the Heaviside step function. In Eq. (4), excitations are associated with displacements of length scale $a$ (of the order of a particle diameter) that persist for a time $\Delta t$ [15]. To get rid of uninteresting short scale motion, we consider positions averaged over a short time scale, $\overline{\mathbf{r}}_i(t) = \delta t^{-1} \int_0^{\delta t} \mathbf{r}_i(t + t')dt'$, with $\delta t$ large enough to suppress short scale fluctuations but still much shorter than relevant hopping times leading to structural rearrangements [43], cf. Ref. [15]. On average, the indicator Eq. (4) will grow linearly with $\Delta t$ as long as this commitment time is larger than the minimal time associated with a persistent displacement (or "instanton time" [15]). This means that we can extract the average concentration of excitations $c_a$ from the average of Eq. (4)

$$\langle C_a(\Delta t)\rangle \approx \Delta t c_a. \qquad (5)$$

To extract the scaling of $c_a$ with pressure, cf. Eq. (1), we consider fixed values of the commitment time for varying pressure. Figure 2 shows $\langle C_a(\Delta t)\rangle$ as a function of $p^* - p_0^*$ in the system with parameters $(N, \nu, \alpha, x_1) = (64 \times 64, 0.780, 1.4, 1/3)$ [44]. In the supercompressed regime,

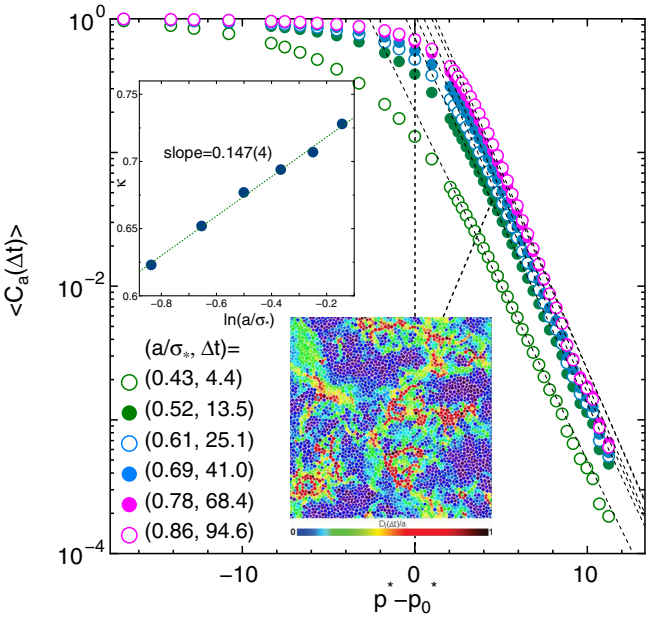


FIG. 2. Averaged excitation indicator $\langle C_a(\Delta t)\rangle$ as a function of pressure $p^* - p_0^*$, for several values of $(a, \Delta t)$ used to define an excitation, for the system with $(N, \alpha, x_1) = (64 \times 64, 1.4, 1/3)$. The inset shows the dependence with $a$ of the parameter $\kappa_a$ obtained from fitting the data with Eq. (1). We also show a typical realization of the displacement field $D_i(\Delta t)$ for the choice $(a/\sigma_*, \Delta t) = (0.52, 13.5)$ that illustrates dynamic heterogeneity in the system at the shown supercompressed conditions.

$p^* > p_0^*$, $\langle C_a\rangle$ decays exponentially over almost 3 orders of magnitude with pressure, in agreement with the prediction of Eq. (1). This behavior is systematic for a range of values of $a$ and $\Delta t$, suggesting that excitations can be identified robustly. Furthermore, the inset to Fig. 2 shows that the rate of decay with pressure in the exponential function, $\kappa_a$ scales logarithmically with the length scale $a$, as predicted by Eq. (2), with each $\kappa_a$ independently obtained from the exponential fits for $p^* > p_0^*$ of the main panel.

In Fig. 2, we also give an illustration of the spatial distribution of excitations, whose facilitated motion gives rise to dynamic heterogeneity. In the figure, we plot an instance of the spatial displacement field $D_i(\Delta t) = |\overline{\mathbf{r}}_i(\Delta t) - \overline{\mathbf{r}}_i(0)|$ for all particles. Mobile particles, $D_i(\Delta t) > a$, are colored dark red, while immobile ones, $D_i(\Delta t) = 0$, dark blue, with disks with intermediate values, $0 < D_i(\Delta t)/a < 1$, colored with a scale between these.

Now, we consider the behavior of the overall relaxation time in the supercompressed regime. We estimate $\tau_\alpha$ from the self-intermediate scattering function $F_s(k,t) = N^{-1}\sum_{i=1}^{N}\langle \exp\{-i\mathbf{k}\cdot[\mathbf{r}_i(t) - \mathbf{r}_i(0)]\}\rangle$ at wave vector $k^* = 2\pi/\sigma_*$. Specifically, we extract $\tau_\alpha$ from $F_s(k^*, \tau_\alpha) = 10^{-1}$. Figure 3 shows the obtained $\tau_\alpha$, in units of $\tau_0 = \tau_\alpha(p_0^*)$, vs $p^*$. For high pressures, we expect the relaxation time to obey Eq. (3). In order to fit both high and low pressures, we use the form

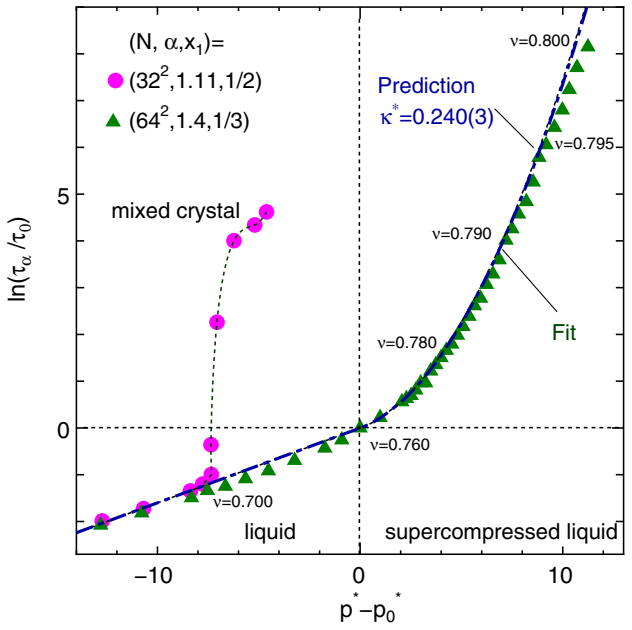


FIG. 3. Structural relaxation time $\ln(\tau_\alpha/\tau_0)$ as a function of $p^* - p_0^*$ for the nonequimolar mixture $(N, \alpha, x_1) = (64 \times 64, 1.4, 1/3)$ as extracted numerically (symbols). We also show a fit with Eq. (6) [dashed line; fitting parameters are $p_0^* = 17.6568(4)$, $\tau_0 = 3.18$, $\kappa = 0.241(4)$, $\lambda = 0.169(4)$]. We also show the time scale that would be predicted by taking $\kappa$ from the excitation data and using Eq. (6) (dotted-dashed line). For comparison with the supercompressed case, we show the data for the equimolar mixture $(N, \alpha, x_1) = (32 \times 32, 1.11, 1/2)$ which crystallizes at these conditions.

$$\ln\left(\frac{\tau_\alpha}{\tau_0}\right) = \begin{cases} e^{\kappa^2(p^*-p_0^*)^2+\lambda(p^*-p_0^*)} & p^* \geq p_0^* \\ e^{\lambda(p^*-p_0^*)} & p^* < p_0^* \end{cases}, \quad (6)$$

where $\kappa$ and $\lambda$ are fitting parameters. Equation (6) interpolates from the low pressure liquid regime to the high pressure supercompressed regime. Equation (6) (dashed line) fits the data (symbols) well, as shown for the system with the nonequimolar mixture $(N, \alpha, x_1) = (64 \times 64, 1.4, 1/3)$, over a range of time scales spanning 4 orders of magnitude. Note that, while for $p^* < p_0^*$ the relaxation time behaves in an "Arrhenius" fashion (in the sense that it appears exponential in $p^*$), for $p^* > p_0^*$ the behavior is "super-Arrhenius." The crossover to super-Arrhenius behavior indicates dominance of heterogeneous dynamics. From Figs. 1–3, we identify the onset pressure $p_0^*$ as the point at which this crossover takes place. That the overall relaxation rate can be accounted for with a parabolic law is another indication of the validity of the DF approach for interpreting the phenomenology of glass forming systems with hard core interactions [45].

The change from Arrhenius to super-Arrhenius behavior in the nonequimolar mixture occurs in the absence of a structural change to either a mixed crystal or due to microcrystallization. To highlight this, we also show, in Fig. 3, the structural relaxation of the equimolar mixture $(N, \alpha, x_1) = (32 \times 32, 1.11, 1/2)$ which does crystallize. In this case, the time suddenly increases around $p^* \sim 10$ due to the transition from liquid to mixed crystal, see Fig. 1, in a manner which is quite distinct to that of the supercompressed system. Furthermore, in contrast to the equimolar case at $\alpha = 1.4$, whose freezing packing fraction is $\nu_f \approx 0.77$, for the nonequimolar mixture, there is no freezing point in terms of microcrystallization, at least up to $\nu = 0.80$, see Fig. 1.

The results for the density of excitations, Fig. 2, and for the relaxation time, Fig. 3, provide two independent estimates of the energy scales from Eqs. (1), (2), and (3), respectively. From DF, we would expect that the ratio $\kappa/\kappa^*$, where $\kappa^* = \kappa_{\sigma_*}\sqrt{\gamma/d_f}$, should be $\kappa/\kappa^* \approx 1$, where $d_f = 1.8 \sim 1.9$ is the fractal dimension associated to hierarchical facilitation estimated numerically in Ref. [15] for systems in two dimensions. In the nonequimolar mixture studied, $\kappa \sim 0.241(4)$ from the relaxation time, cf. Fig. 3, while $\kappa^* \sim 0.240(3)$ (in the case of $d_f = 1.9$) from the excitation data, since $(\kappa_{\sigma_*}, \gamma) = [0.748(2), 0.196(5)]$, cf. Fig. 2. The ratio is then $\kappa/\kappa^* = 1.00(2)$ which is close to unity. This means that the relaxation time for pressures above the onset could have been predicted directly from the excitation concentration data using $\kappa^*$ in the parabolic law Eq. (3). The accuracy of this predicted fit is shown in Fig. 3 (dashed-dotted line) [46].

In summary, we have performed extensive numerical simulations of binary hard disk mixtures to study their dynamical properties as a function of pressure. We have shown that the basic predictions of DF theory seem to hold: (i) localized effective excitations, distributed randomly in equilibrium, giving rise to facilitated relaxation; and (ii) average relaxation times grow with increasing compression as the exponential of a quadratic function of pressure. A key aspect of our study is the access to true equilibrated systems at all conditions studied by means of novel event-driven algorithms. Being able to precisely identify the four existing equilibrium phases allowed us to study relaxation in the true supercompressed regime by considering nonequimolar mixtures that do not phase separate or undergo microcrystallization at the high pressures considered.

As for systems with soft interactions [15,16], we have shown, here, that the basic aspects of DF theory seem to apply to systems with hard-core potentials in the regime where relaxation is slow, cooperative, and heterogeneous. In future work, it would be important to test prediction (iii) relating to the existence of trajectory space transitions to inactive dynamical phases. Interesting questions relate to whether such inactive phases display structural features associated to disordered packings of hard objects, such as hyperuniformity [47,48], and to the connection between nonergodic inactive states and glasses obtained by standard compression, cf. [49].

M. I. was supported by JSPS KAKENHI Grant No. JP26400389. Part of the computations were performed

using the facilities of the Supercomputer Center, ISSP, University of Tokyo. D. C. was supported in part by a grant from the U.S. National Science Foundation. A. S. K. was supported by the Director, Office of Science, Office of Basic Energy Sciences, and by the Division of Chemical Sciences, Geosciences, and Biosciences of the U.S. Department of Energy at LBNL, by the Laboratory Directed Research and Development Program at LBNL under Contract No. DE-AC02-05CH11231. J. P. G. was supported by EPSRC Grant No. EP/K01773X/1.

*isobe@nitech.ac.jp

[1] M. D. Ediger, C. A. Angell, and S. R. Nagel, Supercooled liquids and glasses, J. Phys. Chem. **100**, 13200 (1996).
[2] K. Binder and W. Kob, *Glassy Materials and Disordered Solids* (World Scientific, Singapore, 2005).
[3] V. Lubchenko and P. G. Wolynes, Theory of structural glasses and supercooled liquids, Annu. Rev. Phys. Chem. **58**, 235 (2007).
[4] D. Chandler and J. P. Garrahan, Dynamics on the way to forming glass: bubbles in space-time, Annu. Rev. Phys. Chem. **61**, 191 (2010).
[5] L. Berthier and G. Biroli, Theoretical perspective on the glass transition and amorphous materials, Rev. Mod. Phys. **83**, 587 (2011).
[6] G. Biroli and J. P. Garrahan, Perspective: The glass transition, J. Chem. Phys. **138**, 12A301 (2013).
[7] J. P. Garrahan and D. Chandler, Geometrical Explanation and Scaling of Dynamical Heterogeneities in Glass Forming Systems, Phys. Rev. Lett. **89**, 035704 (2002).
[8] J. P. Garrahan and D. Chandler, Coarse-grained microscopic model of glass formers, Proc. Natl. Acad. Sci. U.S.A. **100**, 9710 (2003).
[9] M. Merolle, J. P. Garrahan, and D. Chandler, Space-time thermodynamics of the glass transition, Proc. Natl. Acad. Sci. U.S.A. **102**, 10837 (2005).
[10] J. P. Garrahan, R. L. Jack, V. Lecomte, E. Pitard, K. van Duijvendijk, and F. van Wijland, Dynamical First-Order Phase Transition in Kinetically Constrained Models of Glasses, Phys. Rev. Lett. **98**, 195702 (2007).
[11] F. Ritort and P. Sollich, Glassy dynamics of kinetically constrained models, Adv. Phys. **52**, 219 (2003).
[12] J. Jäckle and S. Eisinger, A hierarchically constrained kinetic Ising model, Z. Phys. B **84**, 115 (1991).
[13] P. Sollich and M. R. Evans, Glassy Time-Scale Divergence and Anomalous Coarsening in a Kinetically Constrained Spin Chain, Phys. Rev. Lett. **83**, 3238 (1999).
[14] Y. S. Elmatad, D. Chandler, and J. P. Garrahan, Corresponding states of structural glass formers, J. Phys. Chem. B **113**, 5563 (2009).
[15] A. S. Keys, L. O. Hedges, J. P. Garrahan, S. C. Glotzer, and D. Chandler, Excitations Are Localized and Relaxation Is Hierarchical in Glass-Forming Liquids, Phys. Rev. X **1**, 021013 (2011).
[16] T. Speck and D. Chandler, Constrained dynamics of localized excitations causes a non-equilibrium phase transition in an atomistic model of glass formers, J. Chem. Phys. **136**, 184509 (2012).
[17] C. Dellago, P. G. Bolhuis, and P. L. Geissler, Transition path sampling, Adv. Chem. Phys. **123**, 1 (2002).
[18] P. G. Bolhuis, D. Chandler, C. Dellago, and P. L. Geissler, TRANSITION PATH SAMPLING: Throwing Ropes Over Rough Mountain Passes, in the Dark, Annu. Rev. Phys. Chem. **53**, 291 (2002).
[19] L. O. Hedges, R. L. Jack, J. P. Garrahan, and D. Chandler, Dynamic order-disorder in atomistic models of structural glass formers, Science **323**, 1309 (2009).
[20] T. Speck, A. Malins, and C. P. Royall, First-Order Phase Transition in a Model Glass Former: Coupling of Local Structure and Dynamics, Phys. Rev. Lett. **109**, 195703 (2012).
[21] See, e.g., T. Kawasaki, T. Araki, and H. Tanaka, Correlation between Dynamic Heterogeneity and Medium-Range Order in Two-Dimensional Glass-Forming Liquids, Phys. Rev. Lett. **99**, 215701 (2007); E. Flenner and G. Szamel, Fundamental differences between glassy dynamics in two and three dimensions, Nat. Commun. **6**, 7392 (2015).
[22] The effective diameter $\sigma_*$ can be directly estimated by averaging diameter $\langle\sigma_{ij}\rangle$ for collision pair $(i,j)$ during the EDMD simulation. In the equimolar $(x_1 = 1/2)$ and nonequimolar $(x_1 = 1/3)$ cases, $\sigma_*/\sigma_0$ are estimated as 1.2248(5) and 1.1556(6), respectively.
[23] E. P. Bernard, W. Krauth, and D. B. Wilson, Event-chain Monte Carlo algorithms for hard-sphere systems, Phys. Rev. E **80**, 056704 (2009).
[24] M. Isobe, Simple and efficient algorithm for large scale molecular dynamics simulation in hard disk system, Int. J. Mod. Phys. C **10**, 1281 (1999).
[25] M. Engel, J. A. Anderson, S. C. Glotzer, M. Isobe, E. P. Bernard, and W. Krauth, Hard-disk equation of state: First-order liquid-hexatic transition in two dimensions with three simulation methods, Phys. Rev. E **87**, 042134 (2013).
[26] M. Isobe and W. Krauth, Hard-sphere melting and crystallization with event-chain Monte Carlo, J. Chem. Phys. **143**, 084509 (2015).
[27] M. Isobe, Hard sphere simulation in statistical physics—methodologies and applications, Mol. Simul. **42**, 1317 (2016).
[28] The original SANN algorithm was implemented for 3D; J. A. van Meel, L. Fillion, C. Valeriani, and D. Frenkel, A parameter-free, solid-angle based, nearest-neighbor algorithm, J. Chem. Phys. **136**, 234107 (2012).
[29] To detect a disk belonging to a crystal cluster, we proceed as follows: if a large tagged disk has six nearest neighbors, then, we check the character of these neighbors; if there are more than four large disks which also have six large nearest neighbors, it is categorized as part of a crystal cluster.
[30] J. J. Erpenbeck and W. W. Wood, in *Statistical Mechanics Part B*, Modern Theoretical Chemistry Vol. 6, edited by B. J. Berne (Plenum, New York, 1977), Chap. 1, p. 1.
[31] B. J. Alder and T. E. Wainwright, Phase transition in elastic disks, Phys. Rev. **127**, 359 (1962).
[32] E. P. Bernard and W. Krauth, Two-Step Melting in Two Dimensions: First-Order Liquid-Hexatic Transition, Phys. Rev. Lett. **107**, 155704 (2011).
[33] The mixed crystal is one where particles are located almost on the triangular lattice, as in the monodisperse case, but the

six neighbors of a disk include both large and small particles.

[34] Independent runs of EDMD, instead of ECMC, confirm that the final equilibrium states are the same. The longest simulation length of EDMD is $\mathcal{O}(10^{12})$, which are $10^2 \sim 10^3$ longer than that of past literature.

[35] A. Huerta, V. Carrasco-Fadanelli, and A. Trokhymchuk, Towards frustration of freezing transition in a binary hard-disk mixture, Condens. Matter Phys. **15**, 43604 (2012).

[36] R. J. Speedy, Glass transition in hard disc mixtures, J. Chem. Phys. **110**, 4559 (1999).

[37] K. Froböse, F. Kolbe, and J. Jäckle, Size dependenceof self-diffusion in a dense hard-disc liquid, J. Phys. Condens. Matter **12**, 6563 (2000).

[38] L. Santen and W. Krauth, Absence of thermodynamic phase transition in a model glass former, Nature (London) **405**, 550 (2000).

[39] A. Donev, F. H. Stillinger, and S. Torquato, Do Binary Hard Disks Exhibit an Ideal Glass Transition?, Phys. Rev. Lett. **96**, 225502 (2006).

[40] D. N. Perera and P. Harrowell, Stability and structure of a supercooled liquid mixture in two dimensions, Phys. Rev. E **59**, 5721 (1999).

[41] A. Widmer-Cooper, Structure and dynamics in two-dimensional glass-forming alloys, Ph. D. thesis, University of Sydney, 2006, http://hdl.handle.net/2123/1320.

[42] A. Donev, F. H. Stillinger, and S. Torquato, Configurational entropy of binary hard-disk glasses: Nonexistence of an ideal glass transition, J. Chem. Phys. **127**, 124509 (2007).

[43] Typical trajectories of a tagged disk at supercompressed conditions show that a coarse-graining time of $\delta t = 4.0$, which is about 100 times larger than the mean free time around the transition point in the monodisperse hard disk system, is enough to suppress vibrational fluctuation and is also sufficiently small compared to time scales of disk diffusion from their local trapping cage.

[44] The characteristic time scales $\Delta t$ of the excitations for each $a$ were estimated by preliminary independent runs. In the production runs, the averaged indicator function $\langle C_a(\Delta t)\rangle$ was calculated for each pressure. This allowed us to obtain $\kappa_a$ from a fit to an exponential in the pressure, above the crossover pressure $p_0^*$.

[45] In hard sphere systems, pressure is the appropriate intensive control variable. Nevertheless, the relaxation time is often quoted as a function of the packing fraction. In our case, this can be done by relating $p^*$ to $\nu$ from the phase diagram of Fig. 1. To the extent that one can neglect curvature in the $\nu - p^*$ plot, Eq. (6) will also yield a parabolic law for $\ln \tau_\alpha$ vs $\nu$.

[46] At high packing fractions, $\nu \sim 0.800$, there is a systematic deviation from the DF prediction. Note that there is also a slight deviation from the exponential fit in Fig. 2 in the range $\nu \geq 0.795$ ($p^* - p_0^* \geq 9.2$). This regime is where equilibration is most difficult in simulations, even with the efficient algorithm employed here; these deviations may be an indication of incipient lack of equilibration (which may be more evident in dynamical observables than in the static ones that define the phase diagram of Fig. 1).

[47] A. Donev, F. H. Stillinger, and S. Torquato, Unexpected Density Fluctuations in Jammed Disordered Sphere Packings, Phys. Rev. Lett. **95**, 090604 (2005).

[48] C. E. Zachary, Y. Jiao, and S. Torquato, Hyperuniform Long-Range Correlations are a Signature of Disordered Jammed Hard-Particle Packings, Phys. Rev. Lett. **106**, 178001 (2011).

[49] A. S. Keys, D. Chandler, and J. P. Garrahan, Using the s ensemble to probe glasses formed by cooling and aging, Phys. Rev. E **92**, 022304 (2015).